Desalination 534 (2022) 115781

Contents lists available at ScienceDirect

Desalination

journal homepage: www.elsevier.com/locate/desal

High performance electrospun thin-film composite forward osmosis membrane by tailoring polyamide active layer with polydopamine interlayer for desulfulrization wastewater desalination

Bing Li, Xiao-Xue Ke, Zhi-Hua Yuan, Lu-Bin Zhong, Quan-Bao Zhao, Yu-Ming Zheng *

CAS Key Laboratory of Urban Pollutant Conversion, Institute of Urban Environment Chinese Academy of Sciences, 1799 Jimei Road, Xiamen 361021, China
University of Chinese Academy of Sciences, 19A Yuquan Road, Beijing 100049, China

HIGHLIGHTS

- Polydopamine (PDA) interlayer was prepared on rough & hydrophobic PVDF nanofibers.
- PDA interlayer facilitates the formation of thinner and more cross-linked PA layer.
- Interlayer can alleviate PA defect and improve selectivity of eTFC-FO membrane.
- eTFC-FO with interlayer enhanced performance for high salinity water desalination.

GRAPHICAL ABSTRACT

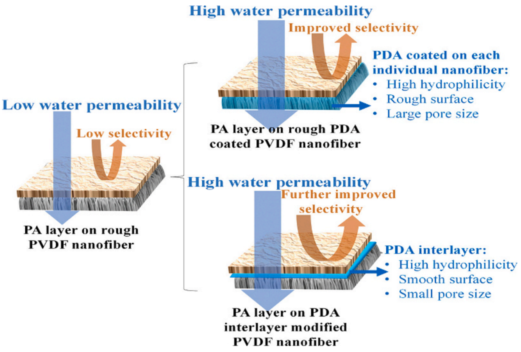

ARTICLE INFO

Keywords:
Desalination
Desulfurization wastewater
Electrospun nanofiber membrane
Forward osmosis
Selectivity

ABSTRACT

The relatively poor selectivity of electrospun nanofiber membrane (ENM) substrate supported thin film composite forward osmosis (eTFC-FO) membranes has hindered their applications. In this study, to overcome the high roughness and large pore size of ENM substrate, a smooth and hydrophilic polydopamine (PDA) interlayer was fabricated on a polyvinylidene fluoride (PVDF) ENM, which was found to be favourable for the formation of a thinner, more cross-linked and less defective polyamide (PA) active layer on the ENM substrate. Desalination tests proved the great effectiveness of PDA interlayer on performance improvement for the eTFC-FO membrane. A quite high water flux (43.0 LMH) and ions rejection (>97.0%) were achieved for a real desulfurization wastewater desalination tested in FO mode. The alleviated PA defects by the PDA interlayer could greatly improve the selectivity. As a comparison with PDA interlayer, PDA coating on each individual nanofiber inside the PVDF ENM substrate was also prepared for eTFC-FO membrane, which would not overcome the disadvantages of rough and large pore sized ENM substrate for PA preparation. Mechanisms of PA formation and performance improvement were detailly discussed in this work.

---

* Corresponding author at: CAS Key Laboratory of Urban Pollutant Conversion, Institute of Urban Environment Chinese Academy of Sciences, 1799 Jimei Road, Xiamen 361021, China.

E-mail address: ymzheng@iue.ac.cn (Y.-M. Zheng).

https://doi.org/10.1016/j.desal.2022.115781
Received 26 September 2021; Received in revised form 8 April 2022; Accepted 8 April 2022

1. Introduction

In recent decades, osmotic pressure driven forward osmosis (FO) has emerged as a promising membrane technique, due to the advantages of low energy consumption and moderate fouling propensity [1–4]. These advantages make FO quite suitable to couple with membrane distillation (MD) or reverse osmosis (RO) for high salinity water desalination [5,6], such as desalination of seawater, brackish water and other high salinity wastewater [7]. However, the performance of a typical thin film composite FO (TFC-FO) membrane was greatly limited by internal concentration polarization (ICP), which occurs inside the substrate and can deteriorate the effective osmotic pressure a lot [8]. Thus, a suitable substrate for a TFC-FO membrane is critical for its wider applications. Numerous FO researches have proved that a desirable substrate for a TFC-FO membrane should be thin, porous and less tortuous to alleviate the ICP [8,9], as well as be hydrophilic for more available pores, of which the substrate could be well wetted during long term FO operation [10,11].

In last decade, electrospun nanofiber membranes (ENMs) has been a promising class of substrates for TFC-FO membranes due to its low thickness, high porosity and interconnected pore structure. And many works proved that the ENMs as substrates can greatly improve the water permeability and lower down the ICP for electrospun TFC-FO membranes (eTFC-FO) [12–16]. However, some main challenges remained in these studies. One is the contradiction between hydrophilic and hydrophobic nanofibers, which would either harm the structure integrity due to the swelling of hydrophilic nanofiber or deteriorate water flux due to hydrophobicity and unavailable pores [14–16]. The other one is the difficulty to prepare defect-free polyamide (PA) layers on rough and large pore sized ENMs, leading to the formation of defective PA layer or even PA layer deformation [16–23]. It was considered that poor selectivity of eTFC-FO membrane seems to be more harmful to performance due to the increased adverse reverse solute diffusion and thus elevated ICP [24,25].

Polydopamine (PDA) is a famous kind of bio-inspired hydrophilic material which can easily adhere onto many materials by self-polymerization [26,27]. And effects of PDA have been proved to improve the performance of TFC-FO membranes based on substrates via both phase inversion [21,22] and electrospinning methods [23]. For TFC-FO membranes with substrates via phase inversion, PDA could be easily coated onto the smooth substrate and PA surface to improve hydrophilicity and antifouling of the membranes [21,22]. However, for ENMs based eTFC-FO, research interests were more focused on PDA coating onto each individual nanofiber inside substrate rather PDA interlayer [25,26], because of the difficulty of PDA interlayer preparation on large pore sized ENMs. And an interlayer in a TFC-FO membrane was found to be effective to alleviate the PA defects, especially for the large pore sized substrates [28–33]. The adhesive PDA was popular to be used as single PDA interlayer or composited with other organic or inorganic materials [29]. On the other hand, recent studies revealed that an interlayer between the PA and substrate layer, such as hydrophilic interlayers [29], could also regulate the interfacial polymerization (IP) process by enhancing amine storage in substrate or interlayer, controlling amine diffusion and regulating nuclei formation [28–30]. Thus, a PDA interlayer on ENM should be promising to provide a high selectivity for an eTFC-FO membrane. However, PDA interlayer was not well studied for the electrospun nanofiber supported TFC membranes. To the best of the authors' knowledge, the only PDA interlayer on ENMs for eTFC-FO was by Yao's group, in which a PDA nanoparticle interlayer was prepared onto hydrophilic polyacrylonitrile (PAN) ENMs via vacuum filtrating [23]. More deep studies on PDA interlayer for eTFC-FO should be carried out. In order to overcome the poor selectivity of eTFC-FO membrane and maintain its high water permeability, a new method to prepare uniform PDA interlayer is needed.

In this study, a PDA interlayer was introduced on a hydrophobic PVDF ENM substrate to prepare high performance eTFC-FO membrane. The PDA interlayer would provide a hydrophilic, smooth surface with decreased pore size, which is favourable for the formation of a thinner and more cross-linked PA layer [13,14]. As a comparison with PDA interlayer, another PDA coating was prepared onto PVDF ENM substrate for eTFC-FO membrane, of which the PDA was coated onto the surface of each individual nanofiber inside the substrate. For performance evaluation, three feed solutions (FSs) were used for desalination tests, including deionized (DI) water, 0.5 M NaCl solution and real desulfurization wastewater from a coal-fired power plant. Desulfurization wastewater is a kind of high salinity wastewater, in which the contaminants were mainly inorganic salts with trace heavy metal ions [34]. The desalination performance of FO process for seawater has been widely studied [35], but the performance of FO process for desulfurization wastewater desalination has seldom been explored. Mechanisms of PA formation and performance improvement of the studied membranes were also discussed according to the characterization and performance tests in this work.

2. Materials and methods

2.1. Materials

PVDF ($M_w = 800{,}000$ g/mol) was purchased from Solvay (France). *N,N*-dimethylformamide (DMF, 99%), isopropanol (IPA, 99%), acetone (99%) and sodium chloride (NaCl) were obtained from Sinopharm Chemical Reagent Co., Ltd. (Shanghai, China). Dopamine (DA, 99%), sodium dodecyl sulfate (SDS, 99%) *M*-phenylenediamine (MPD, 99%) and 1,3,5-trimesoyl chloride (TMC, 98%) were purchased from Sigma-Aldrich. Tris-hydrochloride (tris-HCl, 1 M) was offered by Biosharp (China). DI water was prepared by a lab-scale system. All the chemicals were of analytical grade and used without any further purification.

2.2. Membrane preparation

Fig. 1 shows the process to fabricate the eTFC-FO membranes, which can be divided into three steps: electrospinning process, PDA modification process and PA layer fabrication process.

2.2.1. Preparation of PVDF ENMs

The PVDF ENMs were prepared by an electrospinning technique. PVDF powder was firstly dissolved in a DMF/acetone (volume ratio, 1:1) mixture, and stirred vigorously at 70 °C for 6 h until a uniform 10 w/v% PVDF solution was obtained. The PVDF solution was degassed at room temperature overnight. The addition of acetone into the solution was for a higher solvent volatility during the electrospinning process. Briefly, a 9.6 mL PVDF solution was electrospun onto a piece of silicon paper in 8 h at a tip-collector distance of 15 cm and a voltage of 15 kV. The nascent PVDF ENM was then heat pressed by a paper laminator (No.3893, Deli, China) and dried at 50 °C for at least 72 h before use.

2.2.2. PDA modification of PVDF ENMs

The PDA interlayer modified substrate was denoted as SC (Substrate Surface Coating) substrate, and the substrate with PDA coating onto each individual nanofiber was denoted as NC (Individual Nanofiber Surface Coating) substrate. Both the SC and NC PDA coatings were prepared by the self-polymerization of 2 g/L dopamine (DA) in 0.1 M Tris-HCl buffer solution (pH = 8.8). Before NC coating process, the PVDF ENMs were pre-wetted with IPA for 60 s and washed with a large amount of DI water for several times, while no pre-wetting process were carried out for SC coating. For the IPA pre-wetted ENMs, DA monomer can diffuse into the available pores of ENMs and form uniform PDA coating onto each individual nanofiber surface (NC PDA). For the ENMs without pre-wetting, DA can only attach to the ENMs surface instead of diffusing inside the ENMs. Thus, DA can be polymerized and extend to form a PDA thin film on the ENMs surface (SC PDA).

After certain hours, the DA solution was drained off and the nascent

SCx and NCx ENMs were rinsed with DI water to terminate the self-polymerization reaction, where the x is the PDA treating time.

2.2.3. Preparation of PA active layer

PA active layers were prepared by an IP technique. All the ENMs substrates were pre-wetted with IPA for 60 s and rinsed with DI water for at least three times before IP process, in order to get rid of the deviation of pretreatment. Then, the ENMs were immersed in a 2 wt% MPD aqueous solution with 0.05 wt% sodium dodecyl sulfate (SDS, surfactant) for 2 min. After draining off of MPD solution, the excess MPD solution drops on the ENMs were removed carefully with filter paper. Subsequently, a 0.15 w/v% TMC solution in n-hexane was gently poured onto the ENMs and let be contacted for 1 min to obtain a nascent PA active layer. The as-prepared eTFC-FO membrane was air dried in a fume cupboard for 3 min and cured at 70 °C in air for 10 min. At last, all the prepared eTFC-FO membranes were stored in DI water at 4 °C overnight before any test. The prepared eTFC-FO membranes based on unmodified, SC PDA and NC PDA modified ENMs substrates were respectively referred as eTFC-Pristine, eTFC-SCx, and eTFC-NCx, where x is the PDA coating time in h. Table 1 gives the information of the ENM substrates and the eTFC-FO membranes.

2.3. Characterization

2.3.1. ENMs characterization

Morphology of the ENMs substrates was imaged by a field emission scanning electron microscope (FESEM, S-4800, Hitachi, Japan), and an ImageJ software was used to analyze the fiber diameter [36]. Surface water contact angles (WCAs) of ENMs were characterized by a contact angle analyzer (DSA 100, KRUSS, Germany) at a fixed DI water droplet of 2 μL. The values were measured at 3 different points of each sample and accorded in 60 s [37]. Surface pore sizes of ENMs were analyzed by a porometer 3G machine (Quantachrome Instruments, USA), in which bubble point method was used with a Porofil® wetting fluid (Quantachrome Instruments Co., USA) as the wetting agent. Mechanical properties of the ENMs were characterized by a mechanical machine (AGS-X, Shimadzu, Japan). ENMs thickness was measured by a digital micrometer (Mitutoyo Absolute Corp, Kawasaki, Japan) and 3 different points were measured for each sample. X-ray photoelectron spectroscopy (XPS) (JPS-9010MS, JEOL, Japan) was used to examinate their surface element composition. The roughness of the ENMs was characterized by an atomic force microscopy (AFM) (Aglient, USA) with a peak force tapping mode in air.

Table 1
Information of the ENM substrate and the corresponding eTFC-FO membranes.

ENMs substrate	Pretreatment before coating	PDA coating time (h)	eTFC-FO membrane
Pristine[a]	No pre-wetting	0	eTFC-Pristine[b]
NC2	Pre-wetting with IPA	2	eTFC-NC2
NC4		4	eTFC-NC4
NC6		6	eTFC-NC6
NC8		8	eTFC-NC8
NC10		10	eTFC-NC10
SC2	No pre-wetting	2	eTFC-SC2
SC4		4	eTFC-SC4
SC6		6	eTFC-SC6
sC8		8	eTFC-SC8
SC10		10	eTFC-SC10

[a] Pure PVDF ENM substrate.

[b] eTFC-FO membrane based on pure PVDF ENM substrate.

A gravimetric method was applied to acquire the water uptake and porosity of the ENMs [38,39]. Prior to water uptake tests, the studied ENMs were dried at 50 °C in air for 24 h and weighed (denoted Dry weight as W_{dry}). Then the samples were hang into a 2000 mL flask with 1500 mL DI water at 70 °C for 72 h to ensure their full absorption with water vapor, and weighed the wet weight (W_{wet}). The water uptake% was calculated by Eq. (1):

$$Water\ uptake = \frac{W_{wet} - W_{dry}}{W_{dry}} \times 100\% \tag{1}$$

Similarly, ENMs were also dried at 50 °C for 24 h before porosity tests and the W_{dry} was weighed. Then, the dry samples were immersed in IPA for 24 h to ensure full filling of the inner pores and weighed the W_{wet}. The overall porosity (ε) was then calculated by Eq. (2):

$$\varepsilon = \frac{W_{wet} - W_{dry}}{\rho_{IPA} \times A \times Z} \times 100\% \tag{2}$$

where ρ_{IPA} is the density of IPA, A and Z are the effective area and thickness of the ENMs, respectively.

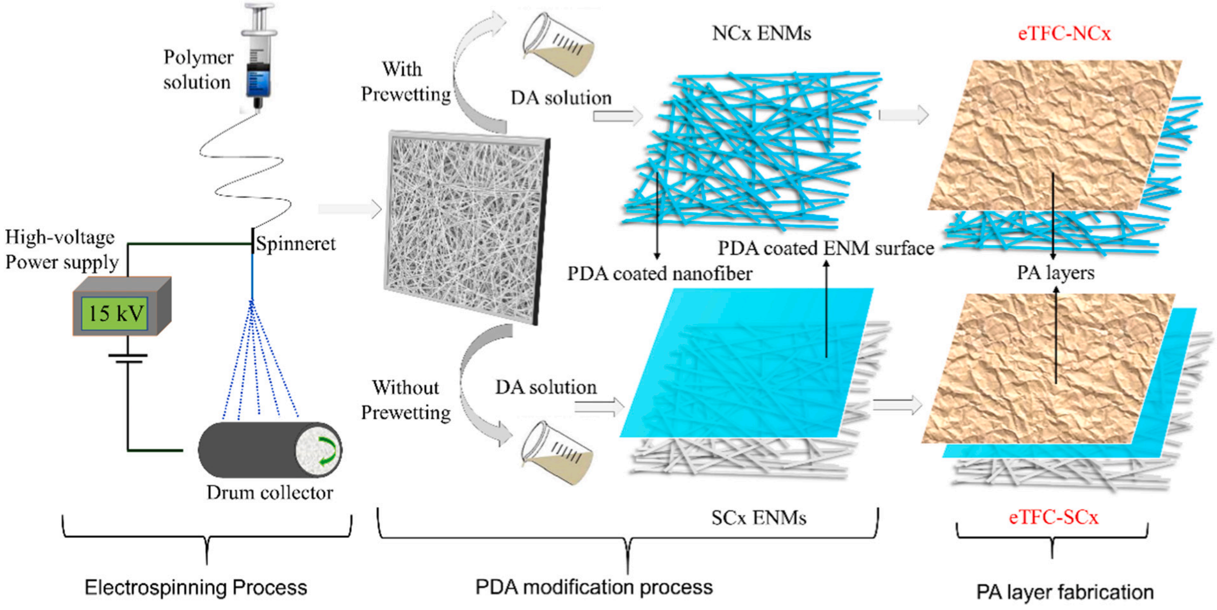

Fig. 1. Preparation process of eTFC-FO membranes, where x in eTFC-SCx and eTFC-NCx is the PDA treating time in h.

2.3.2. PA active layer characterization

The surface and cross-section morphology of the studied eTFC-FO was imaged by FESEM (S-4800, Hitachi, Japan). WCA of PA layers were evaluated by the contact angle analyzer (DSA 100, KRUSS, Germany). The roughness of the PA layer was characterized by an atomic force microscopy (AFM) (Aglient, USA). Attenuated total reflection Fourier transform infrared (ATR-FTIR) and XPS were used to test the chemical composition of PA layer, and the degrees of crosslinking of PA layers were calculated according to the XPS results by Eqs. (3) and (4) [40,41]:

$$Crosslinking = \frac{x}{x+y} \times 100 \tag{3}$$

$$\frac{O}{N} = \frac{3x+4y}{2x+2y} \tag{4}$$

where x and y are the cross-linked and linear portions of the PA, respectively.

2.4. Forward osmosis tests

Three solutions were used as FSs to evaluate the performance of the studied membranes, which were DI water, 0.5 M NaCl solution and real desulfurization wastewater from a coal-fired power plant (Fujian Huadian Kemen Power Generation Co. Ltd). DI water FS was used to test pure water permeability and determine the transport and structural parameters, and 0.5 M NaCl solution and real desulfurization wastewater were used as high salinity water in long time tests for desalination performance. The evaluation of each membrane was conducted by a lab-scale FO system, used in our previous works [42]. In brief, a home-made membrane cell with an exposed membrane area of 12.5 cm^2 was used. Both cross-flow rates of FS and draw solution (DS) were maintained at 250 mL/min.

2.4.1. Performance test with pure water FS

FO mode (active layer faces against FS) and PRO mode (active layer faces against DS) were applied in pure water permeability tests at a 2 L DI water FS and a 2 L 0.5 M NaCl DS, respectively. After stabilized for 20 min, the water flux (J_w) and reverse salt flux (J_s) were recorded for another 30 min and calculated as follows:

$$J_w = \frac{\triangle V}{A_m \times \triangle t} \tag{5}$$

$$J_s = \frac{V_t C_t - V_0 C_0}{A_m \times \triangle t} \tag{6}$$

ΔV (L) is the volume of permeated water after certain test time of Δt (h). A_m is the effective membrane area (m^2). C_t and C_0 are the final and initial concentration of FS (g/L). And three specimens were used and averaged for each kind of membrane.

2.4.2. Transport and structural parameters determination

A FO methodology [43] was applied in the transport and structural parameters determination. The determination process was of four continuous FO tests for the same one membrane. Different concentration of DS and DI water FS were used in each stage. The J_w and J_s in each stage were recorded and compared to determine the water permeability coefficient (A), salt permeability coefficient (B) and structural parameter (S) of the membranes. Three specimens of each kind of membrane were used in the four stage tests. The A, B and S parameters were calculated by Eqs. (7) and (8):

$$J_w = A\left\{\frac{\pi_D exp\left(-\frac{J_w S}{D}\right) - \pi_F exp\left(\frac{J_w}{k}\right)}{1+\frac{B}{J_w}\left[exp\left(\frac{J_w}{k}\right) - exp\left(-\frac{J_w S}{D}\right)\right]}\right\} \tag{7}$$

$$J_s = B\left\{\frac{C_D exp\left(-\frac{J_w S}{D}\right) - C_F exp\left(\frac{J_w}{k}\right)}{1+\frac{B}{J_w}\left[exp\left(\frac{J_w}{k}\right) - exp\left(-\frac{J_w S}{D}\right)\right]}\right\} \tag{8}$$

where k is the mass transfer coefficient of the DI water FS ($\rightarrow\infty$). D is the bulk diffusion coefficient of the DS (0.5–2.0 M NaCl, 1.48×10^{-9} m^2/s). π_F and π_D are respective osmotic pressures of the FS and DS. C_D and C_F are the respective concentrations of the FS and DS.

2.4.3. Desalination test with NaCl solution FS

Simulated high salinity water (0.5 M NaCl) was used as FS for desalination performance evaluation. Each test was carried out with an initial 60 min DI water FS test as baseline and a subsequent 180 min 3.0 wt% NaCl FS test. After that, the tested membrane was washed with DI water on both sides for 30 min and evaluate the flux recovery with fresh DS and FS for another 60 min. All tests were carried out with 2.0 M NaCl as DS, of which the concentration was adjusted every 60 min by adding certain amount of 4 M NaCl solution. The mass of permeate were recorded every 10 min and the rejection of NaCl was not exhibited due to the reverse salt flux [44].

2.4.4. Desalination test with real desulfurization wastewater FS

The test procedure was similar with 2.4.3, except the used FS. The information of desulfurization wastewater was listed in Table 2. The rejections were focused on the ions of Ca^{2+}, Mg^{2+} and SO_4^{2-}, and calculated according to Eq. (9). Rejections of Na^+ and Cl^- were not calculated due to the reverse salt flux, of which NaCl would diffuse from DS to FS and influence the accuracy of calculated rejections of Na^+ and Cl^- [44].

$$Rejection = \left(1 - \frac{C_0 V_0 - C_t V_t}{\triangle V C_0}\right) \times 100\% \tag{9}$$

ΔV (L) is the volume of permeated water after certain test time of Δt (h). C_t and C_0 are the final and initial concentrations of Ca^{2+}, Mg^{2+} and SO_4^{2-} in FS (g/L), which were determined by a titration method for each ion. And an ion chromatography method was also used to examine the accuracy of titration method.

3. Results and discussion

3.1. Characterization

3.1.1. ENMs characterization

Fig. S1 shows the surface morphology of the studied PVDF ENMs. The pristine PVDF ENM showed typical randomly arranged nanofibers with a diameter distribution mainly between 350 and 550 nm. This scaffold-like structure invested ENMs with high porosity and interconnected pores, both of which would be favourable for a low ICP of an eTFC-FO membrane. For the SC PDA coated ENMs, the substrate surface was gradually covered with PDA interlayer, whose covering area was in a positive correlation with the PDA treating time. The surface of SC10 ENM was almost all covered by PDA interlayer, which could reduce the undesirable surface roughness and large surface pore size of ENMs a lot. In contrast, all the NC ENMs surfaces were still rough with almost no

Table 2
Composition information of desulfurization wastewater.

pH	Conductivity (mS/cm)	Ca^{2+} (mg/L)	Mg^{2+} (mg/L)	SO_4^{2-} (mg/L)	Cl^- (mg/L)	Others
5.4	27.7	440.1	6803.1	7996.4	10,576.6	Mainly Na^+ and trace heavy meatal ions

changes after modification. The negligible change of nanofiber diameter proved that NC PDA coating was ultrathin and would not change the pore size and overall porosity of NC ENMs. The AFM analysis results of the studied ENMs in Fig. S2 also confirmed the roughness of SCx substrates decreased with the increase of modification time. The NCx substrates showed close roughness with the pristine ENM, which was consistent with the ENMs surface morphology observed in Fig. S1. Besides surface roughness, cross-section SEM images of the studied ENMs were also used to study the morphology change. Fig. S3 demonstrated that the PDA interlayer was ultrathin and well bound with the surface nanofiber of SCx substrates, while no obvious morphology changes were observed in the NCx cross-section images. The morphology difference between SCx and NCx substrates was due to the diffusion of DA monomer during the modification process. For SCx substrate, DA monomer can only attach to the substrate surface rather than the pores inside the substrate without pre-wetting before modification. Thus, a uniform PDA interlayer would be formed and extend with the increase of modification time. For NCx substrate, DA monomer can diffuse into the pores inside the pre-wetted ENMs. As the DA diffusion within the pores was not static, the DA and nascent PDA would move inside the pores until adhere on the surface of each nanofiber. Thus, PDA coating on nanofiber surface was formed rather than a net-like PDA inside the substrates.

Besides the surface morphology, other structural properties of ENMs are also critical to eTFC-FO membranes. It can be observed from Table S1 that there were almost no differences on the thickness (~40 μm), water uptake (1.0%–2.5%) and overall porosity (~80%) between the pristine and modified ENMs. The negligible change of modified ENMs thickness and porosity proved that both PDA coatings were ultrathin. And the slightly increased water uptake due to the hydrophilic PDA coating would not cause significant ENMs swelling in aqueous solution. However, the other properties in showed quite different changes after PDA modification. For SCx substrates in Table S1, its modified surface showed gradually decreased WCA to ~63° when the PDA treating time increased to 10 h. While the other surface remained hydrophobic (~130°), indicating the successful hydrophilicity enhancement by SC PDA coating. Besides, pore size of SCx substrates also decreased from original ~2.0 μm to ~1.20 μm. For NCx substrates, both top and bottom surface showed decreased WCA values with the increase of PDA treating time, as shown in Table S1. When the NC PDA coating time reached 8 and 10 h, NC8 and NC10 substrates showed super hydrophilicity that the water droplet spread so fast to be exactly measured. And all the NCx substrates were of similar pore size with the pristine. The WCA difference between SCx and NCx at the same PDA treating time was attributed to the change of surface roughness and pore size after modification.

Mechanical property is another important indicator for membranes. Fig. 2 shows that the tensile strength and elongation at break of ENMs were both enhanced by SC and NC PDA coatings. Higher mechanical properties can be obtained by longer PDA treating time for both SCx and NCx ENMs. This enhancement may be attributed to the PDA fusion effects on the adjacent nanofibers, compared with the pristine where no connected force was between the nanofibers [45].

The chemical characterization results by XPS in Fig. 3a shows that, only F and C were detected on the pristine PVDF ENM surface without any detection of other elements, indicating the high purity of the PVDF powder used in this work. Whereas, characteristic N and O peaks of PDA were detected after modification. As expected, N and O were detected on the both top and bottom surfaces of NCx ENMs (Fig. 3a and b). In contrast, XPS results of SCx ENMs proved that they were covered by PDA thin film on only one side (Fig. 3a), while the rest nanofibers remained unmodified (Fig. 3b). The detailed XPS information was listed in Table S2, which also confirmed the N and O contents of both SCx and NCx increased with the increase of modification time.

All abovementioned characterization proved that SC and NC coatings were successfully fabricated onto the hydrophobic PVDF ENMs, and the advantages of original PVDF ENMs were remained, including low water uptake, high overall porosity and low thickness. After modification, hydrophilicity of all the SCx and NCx ENMs were enhanced. Meanwhile, SCx ENMs were with much smoother surface and smaller surface pore size, while NCx ENMs surfaces still remained rough and large pore-sized. The effects of the coatings on the formation of PA active layers and FO performance would be discussed in the following.

3.1.2. The eTFC-FO membrane

Before detailed eTFC-FO membranes characterization, FO performance tests of eTFC-SCx and eTFC-NCx as a function of PDA treating time were conducted and optimized.

For eTFC-SCx membranes, their performance was under the comprehensive effects of surface hydrophilicity and surface pore size, as well as the diffusion resistance through SC PDA interlayer. As shown in Fig. 4a, compared with eTFC-Pristine (without modification), the J_w of eTFC-SC2 increased sharply from 18.63 LMH to 60.67 LMH while its J_s/J_w showed a considerable reduction from 0.16 g/L to 0.11 g/L. This performance enhancement indicated the great effectiveness of SC PDA interlayer for a nanofiber supported TFC-FO membrane. With the increase of SC PDA coating time, the selectivity of eTFC-SCx was continually enhanced that the J_s/J_w was as low as 0.05 g/L for eTFC-SC8 and its J_w was gradually decreased to 35.43 LMH. This selectivity increment was probably due to the increase of degree of crosslinking of PA and PA defects alleviation by SC PDA interlayer [21], while its gradually decreased J_w may be due to the transport resistance by PDA interlayer [22]. And further increase of SC coating time to 10 h would result in the decrease of both water flux and selectivity, which may be due to the high diffusion resistance through SC10 PDA coating. Thus, eTFC-SC8 with the best selectivity and considerable water flux enhancement was of the best performance among all the eTFC-SCx membranes.

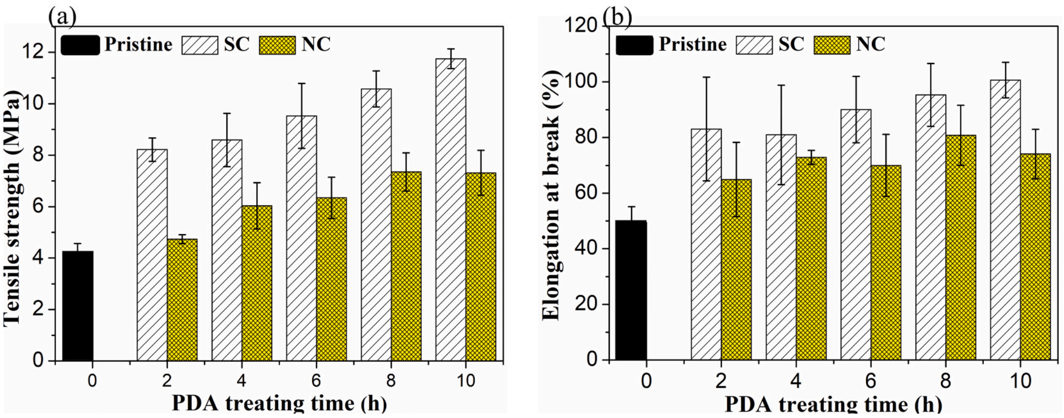

Fig. 2. Mechanical properties of the pristine, SC and NC coated PVDF ENMs: (a) tensile strength, (b) elongation at break.

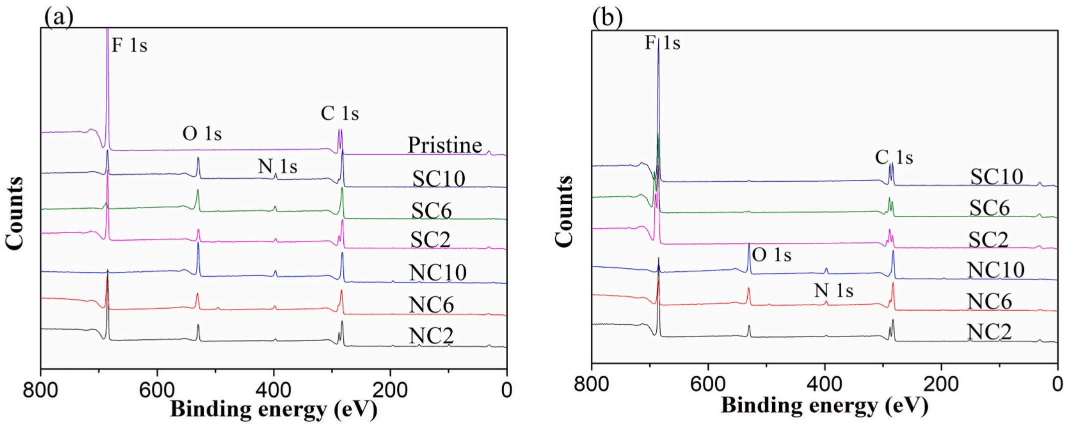

Fig. 3. XPS spectra of the pristine, SC2, SC6, SC10, NC2, NC6 and NC10 PVDF ENMs: (a) top surface analysis of the ENMs and (b) bottom surface analysis of the ENMs.

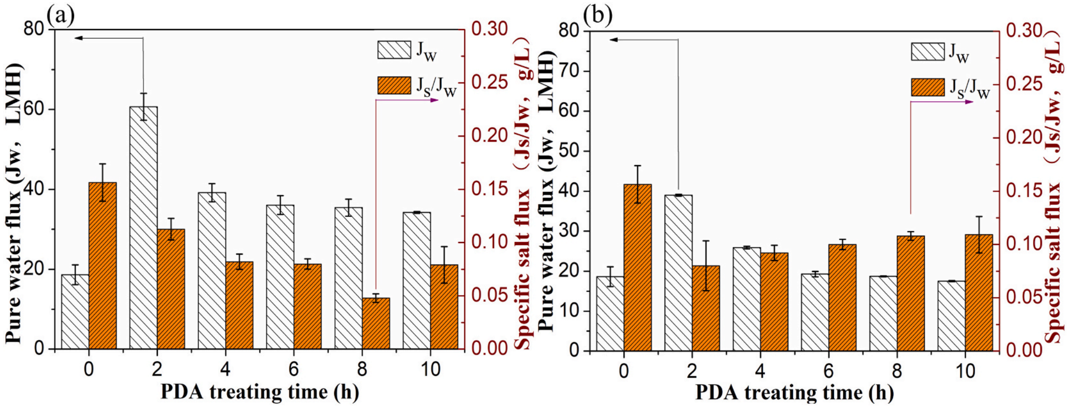

Fig. 4. Effects of PDA treating time on FO performance of (a) eTFC-SCx and (b) eTFC-NCx at DI water FS and 0.5 M NaCl DS, where x is PDA treating time in h.

For eTFC-NCx, the performance was only affected by the change of ENMs hydrophilicity. In Fig. 4b, the eTFC-NC2 showed the best performance with J_w of 39.01 LMH and J_s/J_w of 0.08 g/L among all the eTFC-NCx membranes. Further increase of NC PDA coating time would result in the decrease of both water flux and selectivity, since PA formed on highly hydrophilic ENMs would be deep inside the ENMs pores and defects would be formed [48]. Thus, eTFC-SC8 and eTFC-NC2 were chosen for the rest tests. It seems that their selectivity differences (eTFC-SC8, $J_s/J_w = 0.05$ g/L; eTFC-NC2, $J_s/J_w = 0.08$ g/L) will play a more important role during high salinity water desalination, compared with their close J_w (eTFC-SC8, 35.43 LMH; and eTFC-NC2, 39.01 LMH), which will be discussed in the desalination tests later.

After performance optimization, eTFC-SC8 and eTFC-NC2 were chosen and characterized to investigate the effects of PDA coating on PA active layer formation, compared with the eTFC-Pristine.

Fig. 5 shows the surface and cross section morphology of the chosen membranes analyzed by SEM and AFM. As observed, all the three studied membranes showed typical ridge-valley like PA active layers. The eTFC-Pristine showed a rough and thick PA layer (Fig. 5A1–D1) with no nanofiber imprints due to the convex MPD/TMC interface on hydrophobic PVDF surface. Much smoother and thinner PA active layer of eTFC-SC8 was observed in Fig. 5A2–D2, compared with eTFC-Pristine. No obvious interface between PA layer and PDA interlayer was observed in eTFC-SC8, confirming the great compatibility between PDA interlayer and PA active layer. The great compatibility can be attributed to the reaction between —NH_2 group in PDA with the —COCl in TMC, which has been proved in many other reports and no interface between PDA and PA would be formed [21]. The smoother PA layer should be mainly attributed to the less imprint of the smooth SC8 interlayer and the regulated nuclei formation by smaller surface pore size of substrate. For eTFC-NC2, its PA active layer was even rougher than the eTFC-Pristine, though its PA layer thickness was slightly reduced (Fig. 6A3–D3). This rougher PA layer was caused by the hydrophilic NC2 substrate (WCA, ~75.3°), which would make the MPD/TMC interface deep inside the substrate pores.

For further evidence of the above analysis, physicochemical analyses were conducted for the membranes by ATR-FTIR, XPS and WCA. In Fig. 6a, the ATR-FTIR results showed that all the three eTFC membranes had similar spectra of typical PA. The peaks at 1661 and 1540 cm^{-1} respectively corresponded to the —C═O (amide I) and —N—H (amide II) in PA layer. Peaks at 1611 cm^{-1} attributed to the aromatic ring breathing, and 1410 cm^{-1} was due to the aromatic ring stretching of C═O. The results of ATR-FTIR demonstrated that the PDA modified ENMs substrates for eTFC would not change the chemical nature of PA layer. The weaker peaks of eTFC-SC8 may be caused by its reduced PA thickness. XPS results in Fig. 6b shows that typical elements (C, N and O) of PA were detected in the studied membranes without detection of F, indicating the complete covering of PA layers on the three ENMs substrates.

The detailed XPS results in Table 3 exhibited that both the TFC-SC8 and TFC-NC2 were of lower O/N ratios, 1.38 and 1.35, respectively, which stood for their more cross-linked PA layers [40,41]. For eTFC-NC2, on one hand, the hydrophilic NC2 substrate would increase the amine storage in substrate, which would lead to the more available MPD monomer and be favourable to form a thicker and more cross-linked PA layer [29]. However, on the other hand, hydrogen bond interaction

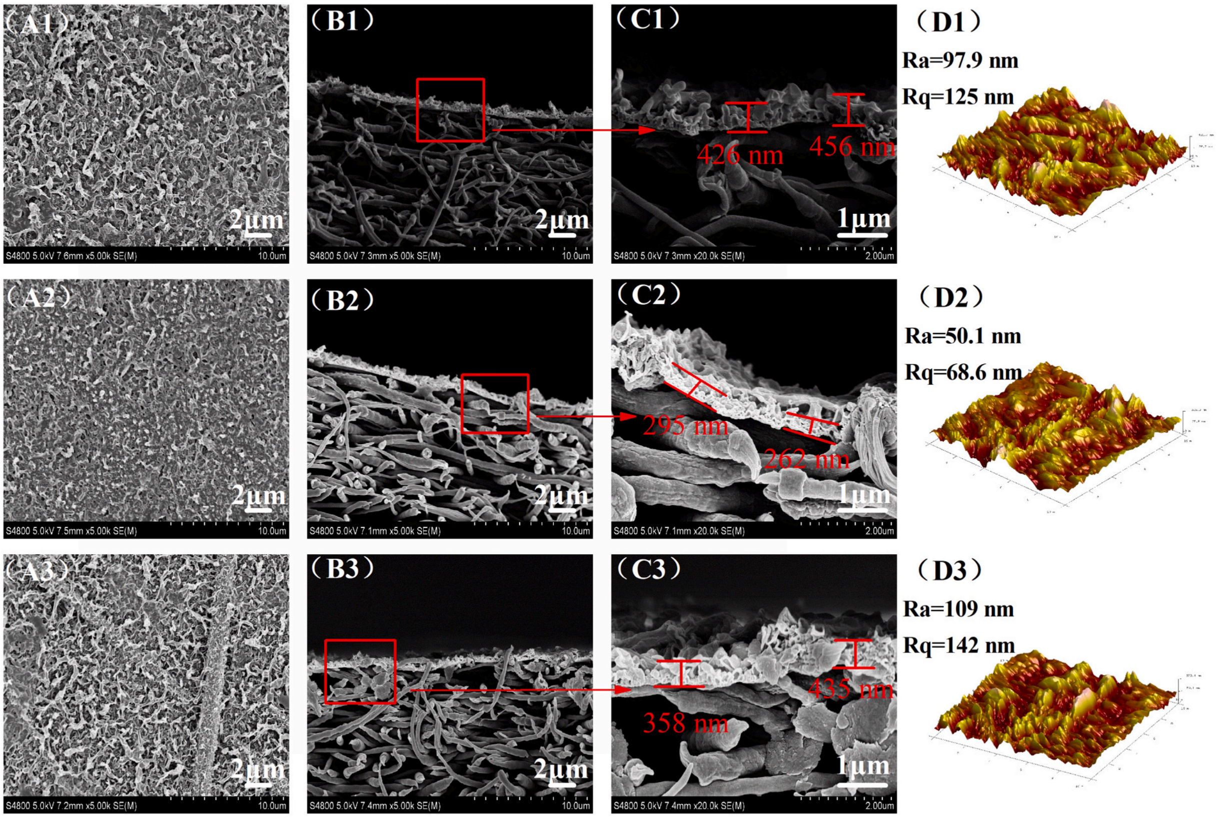

Fig. 5. Surface and cross section morphology observation of the eTFC-Pristine (A1–D1), eTFC-SC8 (A2–D2) and eTFC-NC2 (A3–D3) membranes by SEM and AFM.

between amine monomer and hydrophilic NC2 substrate would lead to the controlled amine diffusion, by which a thinner and less cross-linked PA would be formed [28–30]. Thus, the hydrophilicity of NC2 substrate was controlled at a desirable level, that the resulted PA layer was thinner and more cross-linked under both effects of enhanced amine storage and controlled amine diffusion.

For eTFC-SC8, the substrate has a greater influence on the PA formation compared with that of eTFC-NC2. First, the amine storage in substrate and interlayer would also be enhanced by the hydrophilic PDA interlayer, by which more MPD monomer would be available and lead a more cross-linked PA layer. Second, the amine diffusion from aqueous phase into organic phase would also be controlled by the reduced desorption of MPD from PDA interlayer, which would lead a thinner and less cross-linked PA layer. Third, the smaller surface pore size of SC8 substrate (~1.3 μm) would make the PA nuclei formation along the interlayer, which was favourable to alleviate the PA defects and further enhance the selectivity. Besides, the smooth surface of SC8 would make the formed PA layer smoother by imprint effect [28–30]. Combining with the increased degree of crosslinking of eTFC-SC8 (Table 3), it can also be concluded that amine storage at interlayer or substrate was more important than the controlled amine diffusion. Thus, a thinner and more cross-linked PA layer was formed for eTFC-SC8. And the reduced surface size further contributed to the enhanced selectivity of eTFC-SC8 by PA defects alleviation. Although previous studies reported that the surface coating could simultaneously enhance the transport resistance of water and salt [22], in our study, the PDA interlayer was evidenced that it can positively affect the formation of PA active layer (i.e., higher degree of crosslinking), thus improving the selectively of PA layer.

As an important indicator of hydrophilicity, WCA was under the comprehensive effects of PA morphology and chemical properties. In Fig. 6c, the eTFC-Pristine showed a quite low surface WCA of ~59.0°, which indicated its good wettability. In contrast, the eTFC-SC8 and eTFC-NC2 membranes showed higher WCA values, respective ~101.0° and ~90.0°. This change can be explained by the abovementioned characterization for eTFC. First, as well known, a rougher surface is easier to be wetted [45]. Thus, the eTFC-SC8 with a smoother PA layer would be more difficult to be wetted. Second, the higher degree of crosslinking of eTFC-SC8 meant that more —COCl groups in TMC were reacted with —NH_2 groups in MPD to form less hydrophilic —CO—NH— [45]. As a result, less hydrophilic —COOH and —NH_2 groups would be formed on PA layers. So, it can be concluded that the lowest wettability of eTFC-SC8 was due to its lowest roughness and higher degree of crosslinking. While, the eTFC-NC2 with the highest roughness and improved degree of crosslinking of PA resulted in the second highest wettability next to eTFC-Pristine.

According to all the above characterization, the water permeability improvement of eTFC-NC2 was determined by its reduced PA thickness and higher PA roughness (more permeation area). And its selectivity was enhanced by improved degree of crosslinking of PA. For eTFC-SC8, its enhanced water flux and selectivity should also be contributed to its greatly reduced thickness, improved degree of crosslinking of PA layer, respectively. Although the eTFC-SC8 membrane possess the thinnest PA layer, the additional PDA layer would increase the hydraulic resistance at some extend. Hence, the eTFC-SC8 membrane have similar water permeability with eTFC-NC2 membrane. As the PDA interlayer would not provide selectivity improvement by second rejection [22], the eTFC-SC8 with the highest selectivity should be attributed to the alleviation of PA defects by PDA interlayer, considering its close degree of crosslinking of PA (52.05%) with that of TFC-NC2 (54.77%).

3.2. *Forward osmosis tests*

3.2.1. *Permeability tests with pure water FS*

FO and PRO performance of the studied membranes were conducted with DI water as FS. Compared with eTFC-Pristine in Fig. S4a, the modified eTFC membranes achieved close water flux improvement in

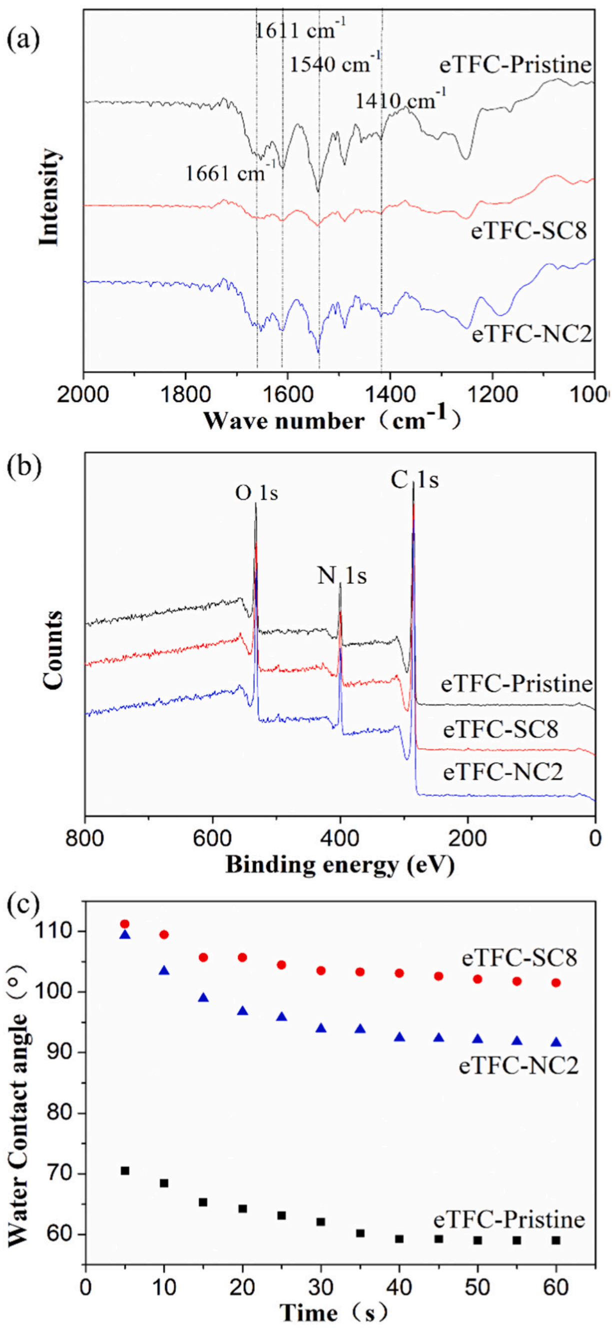

Fig. 6. Surface analysis by (a) ATR-FTIR, (b) XPS and (c) water contact angle for the eTFC-Pristine, eTFC-SC8 and eTFC-NC2 membranes.

Table 3
PA surface chemical composition of the eTFC-Pristine, eTFC-SC8 and eTFC-NC2 obtained by XPS, where ND refers to No Detected.

Sample code	C(at. %)	O(at. %)	N(at. %)	F(at. %)	O/N ratio	Crosslinking %
eTFC-Pristine	75.89	14.78	9.33	ND	1.58	32.19
eTFC-SC8	76.05	13.49	10.46	ND	1.38	52.05
eTFC-NC2	74.84	14.44	10.73	ND	1.35	54.77
Fully cross-linked	75.00	12.50	12.50	–	1.00	100
Fully linear	71.40	19.10	9.5	–	2.00	0

both FO and PRO modes (eTFC-SC8, 35.56/51.11 LMH; TFC-NC2, 38.06/61.18 LMH in FO/PRO mode). But their selectivity in Fig. S4b showed quite difference. Consistent with above discussion, eTFC-SC8 was of the highest selectivity with J_s/J_w as low as 0.05/0.04 g/L in FO/PRO mode due to the highly cross-linked PA layer and PA defect alleviation caused by PDA interlayer. The eTFC-NC2 showed limited selectivity improvement with J_s/J_w of 0.08/0.08 g/L in FO/PRO mode. This selectivity difference between eTFC-SC8 and eTFC-NC2 would be bigger in the following high salinity desalination tests. The detailed performance comparison between this and other works is listed in Table 4.

3.2.2. *Transport and structural parameters determination*

Fig. S5 shows the water flux and specific salt flux at DI water FS and 0.5–2.0 M NaCl DS. And the transport and structural parameters were calculated according to an FO method [43] and were listed in Table 5. As expected, the positive A values of eTFC-SC8 (4.93 LMH/bar) and eTFC-NC2 (5.44 LMH/bar) were much higher than that of the eTFC-Pristine (0.68 LMH), demonstrated with their close water permeability improvement. While the B/A value of eTFC-SC8 (0.07 bar) was lower than that of eTFC-NC2 (0.10 bar), indicating the higher selectivity of eTFC-SC8. However, the S values of eTFC-SC8 (221 μm) and eTFC-NC2 (192 μm) increased compared with eTFC-Pristine (116 μm). This S value increase of eTFC-NC2 was due to the decrease of substrate porosity after PA deposition, which was deep inside its substrate pores due to the MPD/TMC solution intrusion inside the substrate [46]. For eTFC-SC8, its S value increase was caused by the slightly porosity decrease by SC8 PDA coating, as abovementioned in Table S1.

3.2.3. *Desalination test with 0.5 M NaCl solution FS*

Simulated high salinity water (0.5 M NaCl solution) was used as FS to evaluate the membrane desalination performance. In FO mode tests (Fig. 7a), after DI water baseline tests, all the three studied membranes showed stable water flux in 3 h desalination tests at 0.5 M NaCl solution FS, which proved the great advantage of porous PVDF ENMs as substrates for TFC-FO membranes. The close water flux of eTFC-SC8 (~34.9 LMH) and eTFC-NC (~35.8 LMH) also confirmed their high water permeability, compared with the eTFC-Pristine (~26.3 LMH).

In the PRO mode, the water flux showed completely different change rules. As shown in Fig. 7b, the initial water flux of the membranes followed the normal permeability order of eTFC-SC8 (34.4 LMH) ≈ eTFC-NC2 (33.9 LMH) > eTFC-Pristine (26.8 LMH) at the early desalination stage. However, the water flux of eTFC-SC8 constantly decreased in the rest test time from 34.4 LMH to 24.8 LMH, of which ending water flux was even lower than that of eTFC-Pristine (26.3 LMH). In contrast, the water flux of eTFC-NC2 remained stable. The constantly decreased PRO

Table 4
FO/PRO performance comparison in this and other works (DI water as FS).

Membrane codes	DS (NaCl)	J_w (LMH) (FO/PRO)	J_s (gMH) (FO/PRO)	J_s/J_w (g/L) (FO/PRO)	Reference
TFC-0.75 (nylon6,6 ENM)	1.0 M	21/27	5.2/11.9	0.24/ 0.44	[13]
Composited-TFC-2 (CA/PVDF dual layer ENMs)	0.5 M	31.3/	0.8/	0.03/	[14]
TFC with nylon6,6 coated PVDF ENMs	1.0 M	22/31	3.7/ 13.33	0.17/ 0.43	[15]
TFC-PVDF-PVA	0.5 M	24.8/–	3.3/–	0.13	[20]
PAN-CNTs-2	1.0 M	49.2/ 61.6	7.2/7.7	0.15/ 0.13	[23]
eTFC-SC8	0.5 M	35.56/ 51.11	1.79/ 2.04	0.05/ 0.04	This work
eTFC-NC2	0.5 M	38.06/ 61.18	3.04/ 4.28	0.08/ 0.08	This work

Table 5
Transport and structural parameters in this work.

Sample code	A (LMH/bar)	B (LMH)	B/A (bar)	S (μm)
eTFC-Pristine	0.68	0.19	0.28	116
eTFC-SC8	4.93	0.36	0.07	221
eTFC-NC2	5.44	0.52	0.10	192

water flux of eTFC-SC8 could be due to its overall hydrophobic ENM substrate compared with eTFC-NC2, since SC8 substrate was modified on only one surface. It should be noticed that the eTFC-Pristine with a hydrophobic substrate did not show obvious flux decrease during the 3 h test under PRO mode. This could be due to its lowest initial water flux, of which much less salt would be rejected inside the substrate and thus minor ICP. It can be observed from Fig. 7b that the enhanced hydrophilicity of PDA interlayer was not enough to keep a stable water flux in long term desalination tests, compared with eTFC-NC2. The NaCl accumulated inside the SC8 substrate would cause the increase of ICP constantly, resulting in a decline in water flux. While the NaCl rejection of the studied membranes was not exhibited here due to the influence of reverse salt flux, of which NaCl was used in both FS and DS and NaCl rejection could not be calculated accurately [44].

Besides that, all the studied membranes showed no higher initial PRO water flux than that of their corresponding tests in FO mode. It is well recognized that a TFC-FO membrane would exhibit higher water flux in PRO mode than FO mode at pure water FS [49–51]. This extraordinary phenomenon was also due to the rejected NaCl inside the substrates in PRO mode. For elevated concentration of FS (or decreased

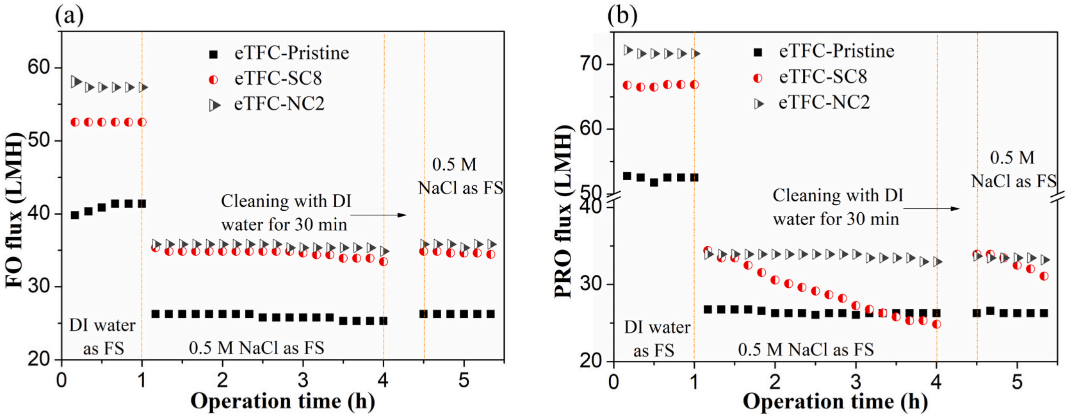

Fig. 7. Desalination performance for 0.5 M NaCl solution of the eTFC-Pristine, eTFC-SC8 and eTFC-NC2: (a) FO water flux and (b) PRO water flux (all tests were at a 0.5 M NaCl FS and a 2.0 M NaCl DS, and DS concentration was controlled every hour).

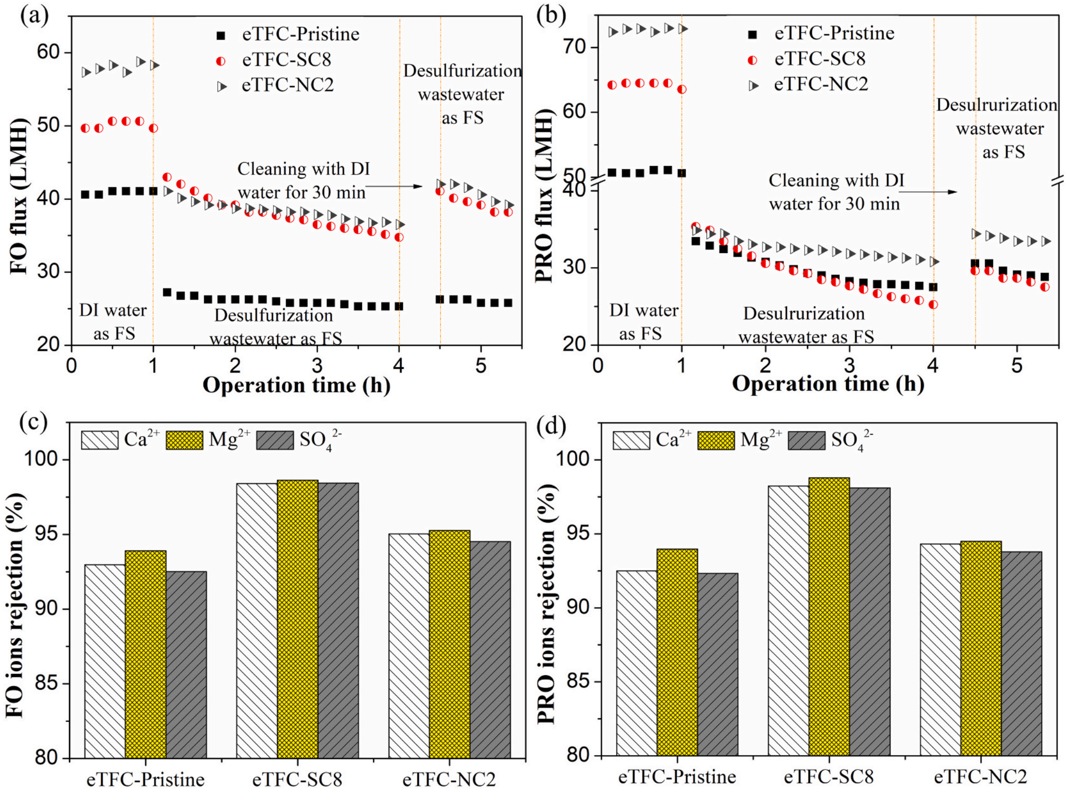

Fig. 8. Desalination performance of the eTFC-Pristine, eTFC-SC8 and eTFC-NC2 membranes for desulfurization wastewater: (a) FO water flux, (b) PRO water flux, (c) FO rejections of ions and (d) PRO rejections of ions (all tests were at a 2.0 M NaCl DS, and DS concentration was controlled every hour).

concentration of DS), the water flux of PRO mode may reduce more significant compared to that in FO mode due to the ICP-enhanced (or ICP-compensated) mechanism [48]. According to this difference between pure water FS and high salinity water FS, FO mode seems to be a better choice than PRO mode for high salinity water desalination or other wastewater purification. It was because that the rejected contaminants at PA surface in FO mode can be alleviated by cross-flow and easier to be removed by membrane washing, compared with the rejected contaminants inside the substrate in PRO mode [47]. Although the 0.5 M NaCl as FS showed insignificant fouling phenomenon, the decreased water flux caused by the enhanced ICP was also a serious problem for an TFC-FO membrane, especially in PRO mode.

3.2.4. *Desalination tests with desulfurization wastewater*

For further evidence of the above discussion in Section 3.2.3, as well as to study the desalination performance for real high salinity wastewater, desulfurization wastewater was used as FS, and the results are shown in Fig. 8. This desalination tests were concentrated on the rejections of the main ions, including Ca^{2+}, Mg^{2+} and SO_4^{2-}. Similarly, the rejections of Cl^- and Na^+ were not concerned due to the reverse salt flux [44].

In Fig. 8a, eTFC-SC8 and eTFC-NC2 exhibited close FO water flux in 3 h desalination process for desulfurization wastewater, both of which were much higher than the eTFC-Pristine. The eTFC-SC8 showed highest FO rejections for all studied ions among the three membranes, which were all higher than 97.0% (Fig. 8c). Besides, FO flux of both eTFC-SC8 and eTFC-NC2 were higher than their corresponding FO desalination tests for 0.5 M NaCl (44.0 mS/cm) in Section 3.2.3, due to the higher driven osmotic pressure at relatively lower concentration of desulfurization wastewater (27.7 mS/cm). However, both eTFC-SC8 and eTFC-NC2 showed slight FO water flux decrease, while the water flux of eTFC-Pristine kept stable. Compared with their stable FO water flux in 0.5 M NaCl desalination, this decrease was due to the membrane fouling on PA active layers by real desulfurization wastewater. The rejected Ca^{2+}, Mg^{2+} and SO_4^{2-} at PA surface would be easier to form scale due to the external concentration polarization (ECP). The eTFC-Pristine with the lowest FO water flux would suffer the lowest PA fouling and remain the most stable FO water flux. As the alleviation by cross-flow, the ECP caused scale was not too serious to result in much water flux decrease for eTFC-SC8 and eTFC-NC2. Considering the high water flux recoveries after membrane washing, it was also confirmed that the membrane fouling in FO mode would not affect the practical application of eTFC-SC8 and eTFC-NC2 in real wastewater desalination, especially for highly selective and smooth eTFC-SC8.

For PRO tests in Fig. 8b and d, the eTFC-SC8 also showed the best selectivity with rejections higher than 97.0% for all the concerned ions, which were much higher than eTFC-Pristine and eTFC-NC2. However, its PRO water flux exhibited the most serious decrease, despite its close initial flux with eTFC-NC2. The decrease of PRO water flux of eTFC-SC8 may be caused by the rejected ions and possible fouling inside the hydrophobic substrate of eTFC-SC8. Although the PDA interlayer coated on the surface of eTFC-SC8 substrate was hydrophilic, it was not able to ensure the performance stability of eTFC-SC8 under PRO mode. The eTFC-Pristine with the hydrophobic ENM substrate also suffered serious PRO water flux deterioration, which is a little slighter than eTFC-SC8 due to the lower initial flux, less fouling and smaller structural parameter. In contrast, the eTFC-NC2 showed the slightest PRO water flux deterioration, though it was also serious, under the rejected ions diffusion and fouling alleviation by its hydrophilic substrate. And the relatively lower water flux recoveries of eTFC-SC8 and eTFC-Pristine confirmed that, the fouling inside hydrophobic substrates was hard to remove by membrane washing, compared with the high water flux recovery of eTFC-NC2.

Combining desalination tests at all the three FSs, it can be concluded that the eTFC-SC8 was of the best FO performance, of which the water flux and selectivity were both greatly improved. The smooth PDA interlayer was effective to overcome the difficulty to prepare highly selective PA layers on rough and large pore sized ENMs. The selectivity enhancement was likely to be due to the PA defect alleviation, which was caused by the PDA interlayer, and played an important role in high salinity water desalination. Besides, FO mode was in preference to PRO mode for real FO membrane applications. Although eTFC-NC2 was with the limited selectivity improvement, it also proved the importance of substrate hydrophilicity to the eTFC-FO membrane performance, especially in long time tests and PRO mode.

The authors have attempted to combine the PDA interlayer and hydrophilic ENM substrates, such as the combination of SC8 PDA interlayer and NC2 PDA coating. However, the SC8 interlayer would further grow and make the interlayer less permeable. How to prepare highly selective PA layers on super hydrophilic ENMs still needs further study.

4. Conclusions

In this study, highly selective eTFC-SC8 was successfully prepared on PVDF nanofiber with a smooth PDA interlayer. Its performance improvement was confirmed in the pure water, 0.5 M NaCl solution and real desulfurization wastewater desalination tests. The selectivity of eTFC-SC8 was greatly enhanced by its more cross-linked PA active layer and PA defects alleviation by PDA interlayer, which make eTFC-SC8 applicable in real wastewater desalination. As a comparison, the limited selectivity improvement of eTFC-NC2 proved the difficulty to prepare a fine PA active layer on a rough and large pore sized nanofiber substrate. Besides, FO mode seems to be preferred to PRO mode in real wastewater desalination due to the alleviation of ECP and fouling by cross-flow.

CRediT authorship contribution statement

Bing Li: Conceptualization, Methodology, Investigation, Data analysis, Writing - Original Draft, Funding acquisition, **Xiao-Xue Ke:** Methodology, Data analysis, Writing - review, **Zhi-Hua Yuan:** Data analysis, Writing - review, **Lu-Bin Zhong:** Writing - review, Funding acquisition, **Quan-Bao Zhao:** Writing - review, **Yu-Ming Zheng:** Supervision, Project administration, Conceptualization, Data analysis, Writing - review & editing, Funding acquisition.

Declaration of competing interest

The authors declare that they have no known competing financial interests or personal relationships that could have appeared to influence the work reported in this paper.

Acknowledgements

The authors are greatly thankful to the financial support from the National Natural Science Foundation of China (Grant No. 51978639), the Science and Technology Planning Project of Xiamen City (3502Z20191021) and the Youth Innovation Promotion Association CAS (Grant No. 2019307).

Appendix A. Supplementary data

Supplementary data to this article can be found online at https://doi.org/10.1016/j.desal.2022.115781.

References

[1] S. Phuntsho, H.K. Shon, S. Hong, S. Lee, S. Vigneswaran, A novel low energy fertilizer driven forward osmosis desalination for direct fertigation: evaluating the performance of fertilizer draw solutions, J. Membr. Sci. 375 (2011) 172–181.

[2] A. Bogler, S.H. Lin, E. Bar-Zeev, Biofouling of membrane distillation, forward osmosis and pressure retarded osmosis: principles, impacts and future directions, J. Membr. Sci. 542 (2017) 378–398.

[3] R. Lambrechts, M.S. Sheldon, Performance and energy consumption evaluation of a fertiliser drawn forward osmosis (FDFO) system for water recovery from brackish water, Desalination 456 (2019) 64–73.

[4] B.X. Mi, M. Elimelech, Organic fouling of forward osmosis membranes: fouling reversibility and cleaning without chemical reagents, J. Membr. Sci. 348 (1–2) (2010) 337–345.

[5] B.G. Choi, M. Zhan, K. Shin, S. Lee, S. Hong, Pilot-scale evaluation of FO-RO osmotic dilution process for treating wastewater from coal-fired power plant integrated with seawater desalination, J. Membr. Sci. 540 (2017) 78–87.

[6] L. Chekli, S. Phuntsho, J.E. Kim, J. Kim, J.Y. Choi, J.-S. Choi, S. Kim, J.H. Kim, S. Hong, J. Sohn, H.K. Shon, A comprehensive review of hybrid forward osmosis systems: performance, applications and future prospects, J. Membr. Sci. 497 (2016) 430–449.

[7] T.S. Chung, L. Luo, C.F. Wan, Y. Cui, G. Amy, What is next for forward osmosis (FO) and pressure retarded osmosis (PRO), Sep. Purif. Technol. 156 (2) (2015) 856–860.

[8] B. Kim, G. Gwak, S. Hong, Review on methodology for determining forward osmosis (FO) membrane characteristics: water permeability (A), solute permeability (B), and structural parameter (S), Desalination 422 (2017) 159–182.

[9] M. Kahrizi, R.R. Gonzales, L.X. Kong, H. Matsuyama, P. Lu, J.Y. Lin, S.F. Zhao, Significant roles of substrate properties in forward osmosis membrane performance: a review, Desalination 528 (2022), 115615.

[10] E.L. Tian, H. Zhou, Y.W. Ren, Z.A. Mirza, X.Z. Wang, S.W. Xiong, Novel design of hydrophobic/hydrophilic interpenetrating network composite nanofibers for the support layer of forward osmosis membrane, Desalination 347 (2014) 207–214.

[11] Y.Q. Wang, T.W. Xu, Anchoring hydrophilic polymer in substrate: an easy approach for improving the performance of TFC FO membrane, J. Membr. Sci. 476 (2015) 330–339.

[12] J.M.C. Puguan, H.S. Kim, K.J. Lee, H. Kim, Low internal concentration polarization in forward osmosis membranes with hydrophilic crosslinked PVA nanofibers as porous support layer, Desalination 336 (2014) 24–31.

[13] L.W. Huang, J.R. McCutcheon, Hydrophilic nylon 6,6 nanofibers supported thin film composite membranes for engineered osmosis, J. Membr. Sci. 457 (2014) 162–169.

[14] M. Shibuya, M.J. Park, S. Lim, S. Phuntsho, H. Matsuyama, H.K. Shon, Novel CA/PVDF nanofiber supports strategically designed via coaxial electrospinning for high performance thin-film composite forward osmosis membranes for desalination, Desalination 445 (2018) 63–74.

[15] L.W. Huang, J.T. Arena, J.R. McCutcheon, Surface modified PVDF nanofiber supported thin film composite membranes for forward osmosis, J. Membr. Sci. 499 (2016) 352–360.

[16] M. Tian, C.Q. Qiu, Y. Liao, S.R. Chou, R. Wang, Preparation of polyamide thin film composite forward osmosis membranes using electrospun polyvinylidene fluoride (PVDF) nanofibers as substrates, Sep. Purif. Technol. 118 (2013) 727–736.

[17] Y.Q. Wang, X.Y. Li, C.L. Cheng, Y.B. He, J.F. Pan, T.W. Xu, Second interfacial polymerization on polyamide surface using aliphatic diamine with improved performance of TFC FO membranes, J. Membr. Sci. 498 (2016) 30–38.

[18] P. Kallem, F. Banat, Y.J. Liang, H. Choi, High performance nanofiber-supported thin film composite forward osmosis membranes based on continuous thermal-rolling pretreated electrospun PES/PAN blend substrates, Chemosphere 261 (2020), 127687.

[19] S. Shokrollahzadeh, S. Tajik, Fabrication of thin film composite forward osmosis membrane using electrospun polysulfone/polyacrylonitrile blend nanofibers as porous substrate, Desalination 425 (2018) 68–76.

[20] M.J. Park, R.R. Gonzales, A.W. Ahmedsur, S. Phuntsho, H.K. Shon, Hydrophilic polyvinyl alcohol coating on hydrophobic electrospun nanofiber membrane for high performance thin film composite forward osmosis membrane, Desalination 426 (2018) 50–59.

[21] H.G. Choi, A.A. Shah, S.E. Nam, Y.I. Park, H. Park, Thin-film composite membranes comprising ultrathin hydrophilic polydopamine interlayer with graphene oxide for forward osmosis, Desalination 449 (2019) 41–49.

[22] H. Guo, Z.K. Yao, J.Q. Wang, Z. Yang, X.H. Ma, C.Y.Y. Tang, Polydopamine coating on a thin film composite forward osmosis membrane for enhanced mass transport and antifouling performance, J. Membr. Sci. 551 (2018) 234–242.

[23] F. Luo, J. Wang, Z.K. Yao, L. Zhang, H.L. Chen, Polydopamine nanoparticles modified nanofiber supported thin film composite membrane with enhanced adhesion strength for forward osmosis, J. Membr. Sci. 618 (2021), 118673.

[24] Q.H. She, X. Jin, Q.H. Li, C.Y.Y. Tang, Relating reverse and forward solute diffusion to membrane fouling in osmotically driven membrane processes, Water Res. 46 (7) (2012) 2478–2486.

[25] P.F. Sun, Y.S. Jang, S.Y. Ham, H.S. Ryoo, H.D. Park, Effects of reverse solute diffusion on membrane biofouling in pressure-retarded osmosis processes, Desalination 512 (2021), 115145.

[26] Z.X. Wang, H.C. Yang, F. He, S.Q. Peng, Y.X. Li, L. Shao, S.B. Darling, Mussel-inspired surface engineering for water-remediation materials, Matter 1 (1) (2019) 115–155.

[27] H. Lee, J. Rho, P.B. Messersmith, Facile conjugation of biomolecules onto surfaces via mussel adhesive protein inspired coatings, Adv. Mater. 21 (2009) 431–434.

[28] Z. Yang, P.F. Sun, X.H. Li, B.W. Gan, L. Wang, X.X. Song, H.D. Park, C.Y.Y. Tang, A critical review on thin-film nanocomposite membranes with interlayered structure: mechanisms, recent developments, and environmental applications, Environ. Sci. Technol. 54 (2020) 15563–15583.

[29] R. Dai, J.Y. Li, Z.W. Wang, Constructing interlayer to tailor structure and performance of thin-film composite polyamide membranes: a review, Adv. Colloid Interface Sci. 282 (2020), 102204.

[30] L.E. Peng, Z. Yang, L. Long, S.H. Zhou, H. Guo, C.Y.Y. Tang, A critical review on porous substrates of TFC polyamide membranes: mechanisms, membrane performances, and future perspectives, J. Membr. Sci. 641 (2022), 119871.

[31] M.J. Park, C. Wang, D.H. Seo, R.R. Gonzales, H. Matsuyama, H.K. Shon, Inkjet printed single walled carbon nanotube as an interlayer for high performance thin film composite nanofiltration membrane, J. Membr. Sci. 620 (2021), 118901.

[32] X.J. Song, Y.J. Zhang, H.M. Abdel-Ghafar, E.S.A. Abdel-Aal, M.H. Huang, S. Gul, H. Q. Jiang, Polyamide membrane with an ultrathin GO interlayer on macroporous substrate for minimizing internal concentration polarization in forward osmosis, Chem. Eng. J. 412 (2021), 128607.

[33] P.F. Sun, Z. Yang, X.X. Song, J.H. Lee, C.Y.Y. Tang, H.D. Park, Interlayered forward osmosis membranes with Ti3C2Tx MXene and carbon nanotubes for enhanced municipal wastewater concentration, Environ. Sci. Technol. 55 (2021) 13219–13230.

[34] Z.K. Sun, H.J. Chen, N. Zhao, Y.X. Feng, F.J. Liu, C.J. Cai, G.M. Che, L.J. Yang, Experimental research and engineering application on the treatment of desulfurization wastewater from coal-fired power plants by spray evaporation, J. Water. Process. Eng. 40 (2021), 101960.

[35] Z. Shabani, T. Mohammadi, N. Kasiri, S. Sahebi, Development of high-performance thin-film composite FO membrane by tailoring co-deposition of dopamine and m-phenylenediamine for the Caspian seawater desalination, Desalination 527 (2022), 115577.

[36] A.M. Khalil, A.I. Schäfer, Cross-linked β-cyclodextrin nanofiber composite membrane for steroid hormone micropollutant removal from water, J. Membr. Sci. 618 (2021), 118228.

[37] T.T. Ni, Q.C. Ge, Highly hydrophilic thin-film composition forward osmosis (FO) membranes functionalized with aniline sulfonate/bisulfonate for desalination, J. Membr. Sci. 564 (2018) 732–741.

[38] M. Tian, Y.N. Wang, R. Wang, Synthesis and characterization of novel high-performance thin film nanocomposite (TFN) FO membranes with nanofibrous substrate reinforced by functionalized carbon nanotubes, Desalination 370 (2015) 79–86.

[39] S.J. Kwon, S.H. Park, M.G. Shin, M.S. Park, K. Park, S. Hong, H. Park, Y.I. Park, J. H. Lee, Fabrication of high performance and durable forward osmosis membranes using mussel-inspired polydopamine-modified polyethylene supports, J. Membr. Sci. 584 (2019) 89–99.

[40] O. Akin, F. Temelli, Probing the hydrophobicity of commercial reverse osmosis membranes produced by interfacial polymerization using contact angle, XPSFTIR, FE-SEM and AFM, Desalination 278 (2011) 387–396.

[41] X.Y. Chi, P.Y. Zhang, X.J. Guo, Z.L. Xu, A novel TFC forward osmosis (FO) membrane supported by polyimide (PI) microporous nanofiber membrane, App. Surf. Sci. 427 (2018) 1–9.

[42] S.F. Pan, Y. Dong, Y.M. Zheng, L.B. Zhong, Z.H. Yuan, Self-sustained hydrophilic nanofiber thin film composite forward osmosis membranes: preparation, characterization and application for simulated antibiotic wastewater treatment, J. Membr. Sci. 523 (2017) 205–215.

[43] A. Tiraferri, N.Y. Yip, A.P. Straub, S.R.-V. Castrillon, M. Elimelech, A method for the simultaneous determination of transport and structural parameters of forward osmosis membranes, J. Membr. Sci. 444 (2013) 523–538.

[44] S.R. Chou, L. Shi, R. Wang, C.Y. Tang, C.Q. Qiu, A.G. Fane, Characteristics and potential applications of a novel forward osmosis hollow fiber membrane, Desalination 261 (2010) 365–372.

[45] Y. Yang, Y.L. Xu, Z.J. Liu, H.Y. Huang, X.F. Fan, Y. Wang, Y.X. Song, C.W. Song, Preparation and characterization of high-performance electrospun forward osmosis membrane by introducing a carbon nanotube interlayer, J. Membr. Sci. 616 (2020), 118563.

[46] Z.Y. Zhou, Y.X. Hu, C.H. Boo, Z.Y. Liu, J.Q. Li, L.Y. Deng, X.C. An, High-performance thin-film composite membrane with an ultrathin spray-coated carbon nanotube interlayer, Environ. Sci. Technol. Lett. 5 (2018) 243–248.

[47] C.Y. Tang, Q.H. She, W.C.L. Lay, R. Wang, A.G. Fane, Coupled effects of internal concentration polarization and fouling on flux behavior of forward osmosis membranes during humic acid filtration, J. Membr. Sci. 354 (2010) 123–133.

[48] L.W. Huang, J.T. Arena, S.S. Manickam, X.Q. Jiang, B.G. Willis, J.R. McCutcheon, Improved mechanical properties and hydrophilicity of electrospun nanofiber membranes for filtration applications by dopamine modification, J. Membr. Sci. 460 (2014) 241–249.

[49] E.L. Tian, H. Zhou, Y.W. Ren, X.Z. Wang, S.W. Xiong, Zakaria.a Irza, Novel design of hydrophobic/hydrophilic interpenetrating network composite nanofibers for the support layer of forward osmosis membrane, Desalination 347 (2014) 207–214.

[50] F.Y. Yu, H.T. Shi, J. Shi, K.Y. Teng, Z.W. Xu, X.M. Qian, High-performance forward osmosis membrane with ultra-fast water transport channel and ultra-thin polyamide layer, J. Membr. Sci. 616 (2020), 118611.

[51] N. Widjojo, T.S. Chung, M. Weber, C. Maletzko, V. Warzelhan, A sulfonated polyphenylenesulfone (sPPSU) as the supporting substrate in thin film composite (TFC) membranes with enhanced performance for forward osmosis (FO), Chem. Eng. J. 220 (2013) 15–23.